2022 IEEE 33rd Annual International Symposium on Personal, Indoor and Mobile Radio Communications (PIMRC)

PIMRC 2022 Best Paper Award

DOD-DOA Estimation using MIMO Antenna Arrays with Manifold Extenders

Zhuqing Tang and Athanassios Manikas
Department of Electrical and Electronic Engineering
Imperial College London

***Abstract*—With increasing demands on capacity and heightened user density, it is imperative to propose approaches that exploit and utilise all possible degrees of freedom (DoF) of a MIMO system. This directly translates to increased channel estimation accuracy. With this motivation, in this paper, a novel MIMO antenna array system with a receiver of N antennas that includes a joint estimation of Direction-of-Arrival (DOA) and Direction-of-Departure (DOD) of the desired user in the presence of other multiple access users, is presented. This is achieved by using the concept of the "Manifold Extender" which increases the dimensionality of the observation space of the received vector-signals, and thus increases the DoF from N to NN_{ext} where N_{ext} is the extended dimension. The performance of the receiver is evaluated against the existing spatial-only and virtual receivers by computer simulation studies.**

***Index Terms*—MIMO, degrees of freedom, manifold extender, array signal processing, DOA and DOD estimation**

NOTATION

A, a	Scalar
$\underline{A}$, $\underline{\text{a}}$	Column vector
$\mathbb{A}$	Matrix
$(\cdot)^T$, $(\cdot)^H$	Transpose, Hermitian transpose,
$(\cdot)^*$	Complex conjugate
$\text{vec}(\mathbb{A})$	Column-wise vectorisation of $\mathbb{A}$
$\exp(\underline{A})$	Element by element exponential of $\underline{A}$
$\mathbb{O}_{M\times N}$	$M \times N$ matrix of zeros
$\odot$	Hadamard product
$\otimes$	Kronecker product
$\mathcal{E}\{\cdot\}$	Expectation operator
$\mathbb{I}_N$	$N \times N$ Identity matrix
$\underline{1}_N$	Column vector of N ones
$\underline{0}_N$	Column vector of N zeros
$\mathcal{R}, \mathcal{C}$	Set of real and complex numbers

I. INTRODUCTION

Future communication systems are expected to operate in very high density signal/user environments with high speeds without sacrificing the quality of service. This drives the requirement for future communication systems to deliver higher number of "degrees-of-freedom" (DoF) that will enable the system to detect, resolve and isolate signals from a large number of interfering sources with greater accuracy. Using antenna arrays at both the transmitter and receiver allows a multitude of devices and users communicating with each other at the same time on the same frequency band, possibly within small enclosures. Therefore, the motivation for this paper is to propose a MIMO system/approach to estimate channel parameters of DOA and DOD of the desired user with high accuracy.

In wireless communications, most of the direction finding approaches are concerned with the DOA estimation problem while the DOD estimation has been ignored. DOA estimation has been an important research area with many applications, including wireless communications, radar, sonar, radio astronomy, etc. On the other hand, only a small number of research has focused on the DOD estimation, with the majority of these approaches designed for radar and sonar applications. Although DOD estimation is also important in wireless communications, it has not been extensively investigated.

In the literature, a DOD estimation approach has been proposed in [1] by exploiting the cooperation between the Tx and the Rx. The Tx beamformer rotates its mainlobe then the Rx measures the power level at the output of the Rx beamformer and the DOD is connected to the largest power. Several papers have been proposed for joint estimation of DOD and DOA. For instance, in [2], a Cramer-Rao bound (CRB) based on DOA and DOD using Multi-Mode Antennas is derived, and then a beamformer is presented to estimate the DOA and DOD by minimising this CRB. In [3], the DOD and DOA have been estimated using a Bartlett beamforming method and a SAGE algorithm [4], and it is implemented in a measurement campaign with dual-polarized arrays and assumed a line-of-sight (LoS) environment. In [5], using a single antenna at the transmitter which provides switched transmitting beams, a joint TDOA, DOA-DOD estimation based on a 3D unitary ESPRIT approach is presented. In [6], the transmit and receive auxiliary beam pairs were designed based on a multi-layer pilot structure for estimating DODs and DOAs in dual-polarized MIMO systems. In this paper, the proposed DOD and DOA estimation algorithm is "blind", unlike the systems proposed in [5], [6] which use "pilots". In particular, a novel MIMO multiple-access wireless communication system is proposed which is able to jointly estimate with high accuracy the DOD and DOA of all paths of the desired user based on the concept of the "manifold extender".

The paper is organised as follows. In Section II, the transmitter, channel and receiver models of the system are proposed, and the antenna array received signal is modelled as a function of a virtual-spatiotemporal manifold extender. Based on this modelling, a joint DOD-DOA estimation algorithm is proposed. In Section III, computer simulation studies are presented and this paper is concluded in Section IV.

978-1-6654-8053-6/22/$31.00 ©2022 IEEE

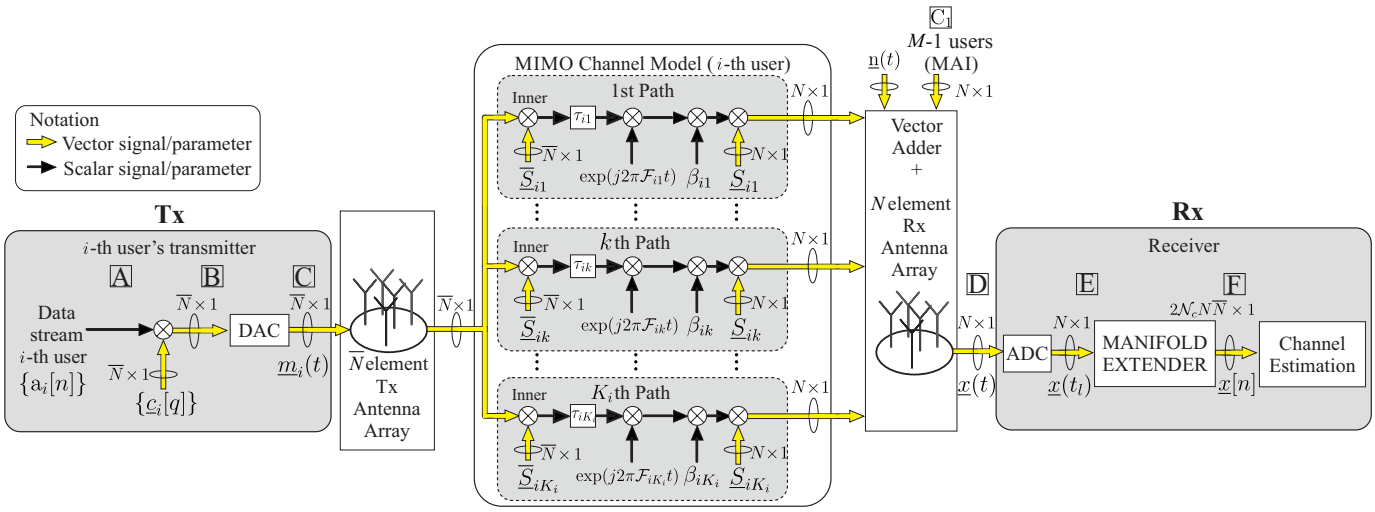

Fig. 1: Baseband representation of the i-th transmitter, the receiver and the MIMO channel. There are M co-channel users: one "desired" with K_i multi-paths plus (M-1) MAI users.

II. System Model

With reference to a multiuser MIMO communication system of M co-channel users, Fig. 1 illustrates the baseband blocks of the i-th user consisting of the transmitter, the channel and the receiver. The transmitter employs an antenna array of $\overline{N}$ elements[1] and it is followed by a frequency selective multiple access noisy channel of K_i resolvable paths. The receiver employs an antenna array of N elements which include a "manifold extender" and a DOA-DOD channel estimator.

A. Transmitter and Channel model

As shown in Fig. 1, M co-channel users including the desired user plus the $M-1$ Multiple Access Interference (MAI) operate at the same time on the same frequency band. The data stream of the i-th user denoted by $\{\mathrm{a}_i[n]\}$ (see point-A in Fig. 1), with a symbol period of T_{cs}, is weighted (point-B) by the known code vector sequence $\{\underline{c}_i[q]\}$ where $\underline{c}_i^T[q]$ is the q-th row of the code matrix $\mathbb{C}_i \in \mathcal{R}^{\mathcal{N}_c \times \overline{N}}$ as this is shown in Fig. 2. The elements of the code matrix $\mathbb{C}_i$ are denoted as $\alpha_{im}[q] \in \{+1,-1\}, \forall m \in [1,\overline{N}], \forall q \in [1,\mathcal{N}_c]$. The vector $\underline{c}_{im}$ denotes the m-th column of $\mathbb{C}_i$ and $\underline{c}_i[q]$ denotes the column version of the q-th row of $\mathbb{C}_i$ which is applied to all Tx antennas at the q-th period T_c with $T_{cs} = \mathcal{N}_c T_c$. At point-B in Fig. 1, the sequence corresponding to the n-th data symbol of the i-th user transmitted across $\overline{N}$ antennas is denoted by the matrix $\mathbb{M}_i[n] \in \mathcal{C}^{\overline{N}\times\mathcal{N}_c}$ and can be written as

$$\mathbb{M}_i[n] = \mathbb{C}_i^T \mathrm{a}_i[n] \tag{1}$$

Finally, using a DAC, the message symbols of Equation 1 become the analogue baseband vector signal $\underline{m}_i(t) \in \mathcal{C}^{\overline{N}\times 1}$ at point-C in Fig. 1. The $\underline{m}_i(t)$ is transmitted via a frequency selective multipath channel of K_i paths, as this is shown in Fig. 1 where the k-th path of the i-th user includes:

[1]Note: a bar at the top of a symbol, e.g. $\overline{N}$, denotes a transmitter's system parameter.

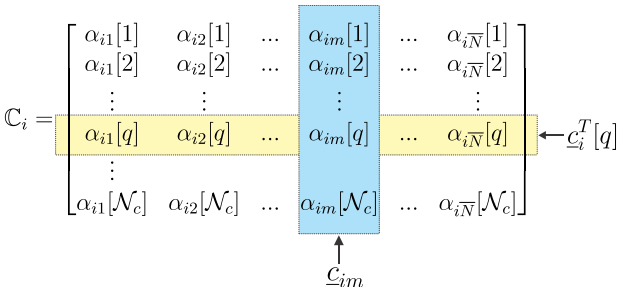

Fig. 2: The code matrix $\mathbb{C}_i$ with elements ± 1 of period $\mathcal{N}_c$.

- the manifold vector $\overline{S}_{ik}$ of the Tx antenna array,
- the delay τ_{ik},
- the Doppler frequency $\mathcal{F}_{ik}$,
- the complex path gain β_{ik},
- the manifold vector $\underline{S}_{ik}$ of the Rx antenna array.

The manifold vectors $\underline{S}_{ik}$ and $\overline{S}_{ik}$ can be expressed as a function of the Cartesian coordinates of the Rx and Tx arrays $[\underline{r}_1, \underline{r}_2, ..., \underline{r}_N] \in \mathcal{R}^{3\times N}$ and $[\overline{r}_1, \overline{r}_2, ..., \overline{r}_{\overline{N}}] \in \mathcal{R}^{3\times \overline{N}}$ as follows

$$\underline{S}_{ik} \triangleq \underline{S}(\theta_{ik})) = \exp(-j\,[\underline{r}_1, \underline{r}_2, ...\underline{r}_N]^T\, \underline{k}(\theta_{ik})) \tag{2a}$$

$$\overline{S}_{ik} \triangleq \overline{S}(\overline{\theta}_{ik})) = \exp(j\,[\overline{r}_1, \overline{r}_2, ..., \overline{r}_{\overline{N}}]^T\, \underline{k}(\overline{\theta}_{ik})) \tag{2b}$$

with $\underline{k} \triangleq \underline{k}(\theta_{ik})$ and $\overline{k} \triangleq \underline{k}(\overline{\theta}_{ik})$ denoting the wavenumber vectors defined as

$$\underline{k} = \frac{2\pi F_c}{c}\,[\cos\theta_{ik},\ \sin\theta_{ik},\ 0]^T \tag{3a}$$

$$\overline{k} = \frac{2\pi F_c}{c}\,[\cos\overline{\theta}_{ik},\ \sin\overline{\theta}_{ik},\ 0]^T \tag{3b}$$

where θ_{ik} and $\overline{\theta}_{ik}$ represent the DOA and the DOD of the i-th user's k-th path, respectively. In addition, F_c denotes the carrier frequency and c is the velocity of light. This parametric channel model allows the modelling of the received array

signal vector $\underline{x}(t)$ at point-D in Fig. 1 to be expressed as a function of channel parameters as

$$\underline{x}(t) = \sum_{i=1}^{M}\sum_{k=1}^{K_i}\beta_{ik}\exp(j2\pi\mathcal{F}_{ik}t)\underline{S}_{ik}\overline{\underline{S}}_{ik}^{H}\underline{m}_i\left(t-\tau_{ik}\right)+\underline{\mathrm{n}}(t) \tag{4}$$

where $\underline{\mathrm{n}}(t)$ is the noise vector which is assumed to be complex white Gaussian noise of zero mean with covariance matrix $\sigma_{\mathrm{n}}^2\mathbb{I}_N$, where σ_{n}^2 is the unknown noise power.

This design of the transmitter is also exploited in [7] which presents a DOD and DOA estimation approach. In this paper, the focus is the design of the receiver to further increase the degrees of freedom of the system and consequently to provide better estimation accuracy. Furthermore, the DOD and DOA estimation comparison with [7] is provided in the computer simulation studies.

B. Receiver model: Virtual-Spatiotemporal Manifold Extender

At point-D in Fig. 1, the received signal vector $\underline{x}(t)$ (given by Equation 4) is firstly discretised with sampling period equal to T_c, producing at point-E the discrete vector $\underline{x}(t_l)$ where t_l denotes the l-th snapshot. Then, these snapshots are fed into a "manifold extender" which transforms the discretised vector $\underline{x}(t_l)\in\mathcal{C}^{N\times 1}$ to a longer snapshot $\underline{x}\,[n]\in\mathcal{C}^{2N\overline{N}\mathcal{N}_c\times 1}$ which we call it a virtual-spatiotemporal snapshot.

In particular, the "manifold extender" block in Fig. 1 collects at its input (point-D) $2\mathcal{N}_c$ snapshots and, for the n-th time interval, forms an $N\times 2\mathcal{N}_c$ matrix $\mathbb{X}\,[n]$. This can be visualised as the n-th slice of the 3D data cube shown in Fig. 3a and modelled as follows (note that, with no loss of generality, the first user is considered to be the desired user):

$$\begin{aligned}\mathbb{X}\,[n] = &\overbrace{\sum_{k=1}^{K_1}\beta_{1k}\underline{S}_{1k}\overline{\underline{S}}_{1k}^{H}\mathbb{T}_{1k}^{T}\mathrm{a}_1\,[n]\exp\left(j2\pi\mathcal{F}_{1k}nT_{cs}\right)}^{\text{desired term}}\\ &+\mathbb{X}_{\mathrm{ISI}}+\mathbb{X}_{\mathrm{MAI}}+\mathbb{N}\,[n]\end{aligned} \tag{5}$$

where $\mathbb{X}_{\mathrm{ISI}}$ and $\mathbb{X}_{\mathrm{MAI}}$ denote the Inter-Symbol Interference (ISI) and the MAI, respectively, expressed as follows

$$\begin{aligned}\mathbb{X}_{\mathrm{ISI}} = &\sum_{k=1}^{K_1}\beta_{1k}\underline{S}_{1k}\overline{\underline{S}}_{1k}^{H}\mathbb{T}_{1k}^{T}\times\\ &\Big\{\mathbb{J}^{\mathcal{N}_c}\mathrm{a}_1\,[n-1]\exp\left(j2\pi\mathcal{F}_{1k}\left(n-1\right)T_{cs}\right)\\ &+\left(\mathbb{J}^{T}\right)^{\mathcal{N}_c}\mathrm{a}_1\,[n+1]\exp\left(j2\pi\mathcal{F}_{1k}\left(n+1\right)T_{cs}\right)\Big\}\end{aligned} \tag{6}$$

$$\begin{aligned}\mathbb{X}_{\mathrm{MAI}} = &\sum_{i=2}^{M}\sum_{k=1}^{K_i}\beta_{ik}\underline{S}_{ik}\overline{\underline{S}}_{ik}^{H}\mathbb{T}_{ik}^{T}\times\\ &\Big\{\mathrm{a}_i\,[n]\exp\left(j2\pi\mathcal{F}_{ik}nT_{cs}\right)\\ &+\mathbb{J}^{\mathcal{N}_c}\mathrm{a}_i\,[n-1]\exp\left(j2\pi\mathcal{F}_{ik}\left(n-1\right)T_{cs}\right)\\ &+\left(\mathbb{J}^{T}\right)^{\mathcal{N}_c}\mathrm{a}_i\,[n+1]\exp\left(j2\pi\mathcal{F}_{ik}\left(n+1\right)T_{cs}\right)\Big\}\end{aligned} \tag{7}$$

In Equation 5, $\mathbb{T}_{ik}\in\mathcal{C}^{2\mathcal{N}_c\times\overline{N}}$ contains the temporal information of the received signal, which is given as

$$\mathbb{T}_{ik} = \mathbb{J}^{l_{ik}}\begin{bmatrix}\mathbb{C}_i\\ \mathbb{O}_{\mathcal{N}_c\times\overline{N}}\end{bmatrix}\odot\left(\underline{\mathcal{F}}_{ik}\underline{1}_{\overline{N}}^{T}\right) \tag{8}$$

with

- $\underline{\mathcal{F}}_{ik}\in\mathcal{C}^{2\mathcal{N}_c\times 1}$ representing the Doppler shift vector within a data symbol, i.e.

$$\underline{\mathcal{F}}_{ik} = \exp\left(j2\pi\mathcal{F}_{ik}\left[0,\ldots,2\mathcal{N}_c-1\right]^{T}T_c\right) \tag{9}$$

- $\mathbb{J}$ is a $2\mathcal{N}_c\times 2\mathcal{N}_c$ matrix defined as follows[2]:

$$\mathbb{J}\triangleq\begin{bmatrix}\underline{0}_{2\mathcal{N}_c-1}^{T}, & 0\\ \mathbb{I}_{2\mathcal{N}_c-1}, & \underline{0}_{2\mathcal{N}_c-1}\end{bmatrix} \tag{10}$$

- $l_{ik}=\left\lfloor\frac{\tau_{ik}}{T_c}\right\rfloor \bmod\mathcal{N}_c$ denoting the discretised delay,
- $\mathbb{N}\,[n]$ representing the noise contribution.

Then, the "manifold extender" block vectorises the matrix to form the $2N\mathcal{N}_c\times 1$ vector $\underline{x}_{\mathrm{st}}[n]$, i.e.

$$\underline{x}_{\mathrm{st}}[n] = \mathrm{vec}\left(\mathbb{X}^{T}\,[n]\right) \tag{11}$$

as this is shown in Fig. 3b. This is further extended to a longer vector with dimensions $2N\overline{N}\mathcal{N}_c\times 1$ (see Fig. 3c) as follows

$$\underline{x}\,[n] = \begin{bmatrix}\left(\mathbb{I}_N\otimes\mathbb{P}_{\mathbb{B}_{11}}^{\perp}\right)\underline{x}_{\mathrm{st}}[n]\\ \left(\mathbb{I}_N\otimes\mathbb{P}_{\mathbb{B}_{12}}^{\perp}\right)\underline{x}_{\mathrm{st}}[n]\\ \vdots\\ \left(\mathbb{I}_N\otimes\mathbb{P}_{\mathbb{B}_{1\overline{N}}}^{\perp}\right)\underline{x}_{\mathrm{st}}[n]\end{bmatrix} \tag{12}$$

where $\mathbb{P}_{\mathbb{B}_{im}}^{\perp}$ denotes the projection operator which isolates the signal corresponding to the m-th Tx antenna of the i-th user, given as

$$\mathbb{P}_{\mathbb{B}_{im}}^{\perp} = \mathbb{I}_{2\mathcal{N}_c}-\mathbb{B}_{im}\left(\mathbb{B}_{im}^{H}\mathbb{B}_{im}\right)^{-1}\mathbb{B}_{im}^{H} \tag{13}$$

with $\mathbb{B}_{im}\in\mathcal{C}^{2\mathcal{N}_c\times K_i(\overline{N}-1)}$ obtained as follows:

$$\begin{aligned}\mathbb{B}_{im} = &\left[\mathbb{J}^{l_{i1}}\begin{bmatrix}\mathbb{C}_{im}\\ \mathbb{O}_{\mathcal{N}_c\times(\overline{N}-1)}\end{bmatrix}\odot\underline{\mathcal{F}}_{i1}\underline{1}_{\overline{N}-1}^{T},\ldots\right.\\ &\left.\ldots,\mathbb{J}^{l_{iK_i}}\begin{bmatrix}\mathbb{C}_{im}\\ \mathbb{O}_{\mathcal{N}_c\times(\overline{N}-1)}\end{bmatrix}\odot\underline{\mathcal{F}}_{iK_i}\underline{1}_{\overline{N}-1}^{T}\right]\end{aligned} \tag{14}$$

Note that the matrix $\mathbb{C}_{im}\in\mathcal{R}^{\mathcal{N}_c\times\overline{N}-1}$ is formed by the codes of the i-th user (see Fig. 2) with the m-th code $\underline{c}_{im}$ of $\mathbb{C}_i$ removed. That is,

$$\mathbb{C}_{im} = \left[\underline{c}_{i1},\ldots,\underline{c}_{i(m-1)},\underline{c}_{i(m+1)},\ldots,\underline{c}_{i\overline{N}}\right] \tag{15}$$

After that, a projection matrix $\mathbb{P}_{\mathbb{B}_1}^{\perp}$ is defined which encloses the projection operators of all Tx antennas of the desired user,

[2]With reference to Equation 10, the power l of $\mathbb{J}$ (or $\mathbb{J}^T$) when applied to a vector $\underline{z}\in\mathcal{C}^{\mathcal{N}_c\times 1}$ or matrix $\mathbb{Z}$, i.e. $\mathbb{J}^l\underline{z}$ $\left(\text{or }\left(\mathbb{J}^T\right)^l\underline{z}\right)$ and $\mathbb{J}^l\mathbb{Z}$ $\left(\text{or }\left(\mathbb{J}^T\right)^l\mathbb{Z}\right)$, downshifts (or upshifts) the vector $\underline{z}$ or matrix $\mathbb{Z}$ by l elements

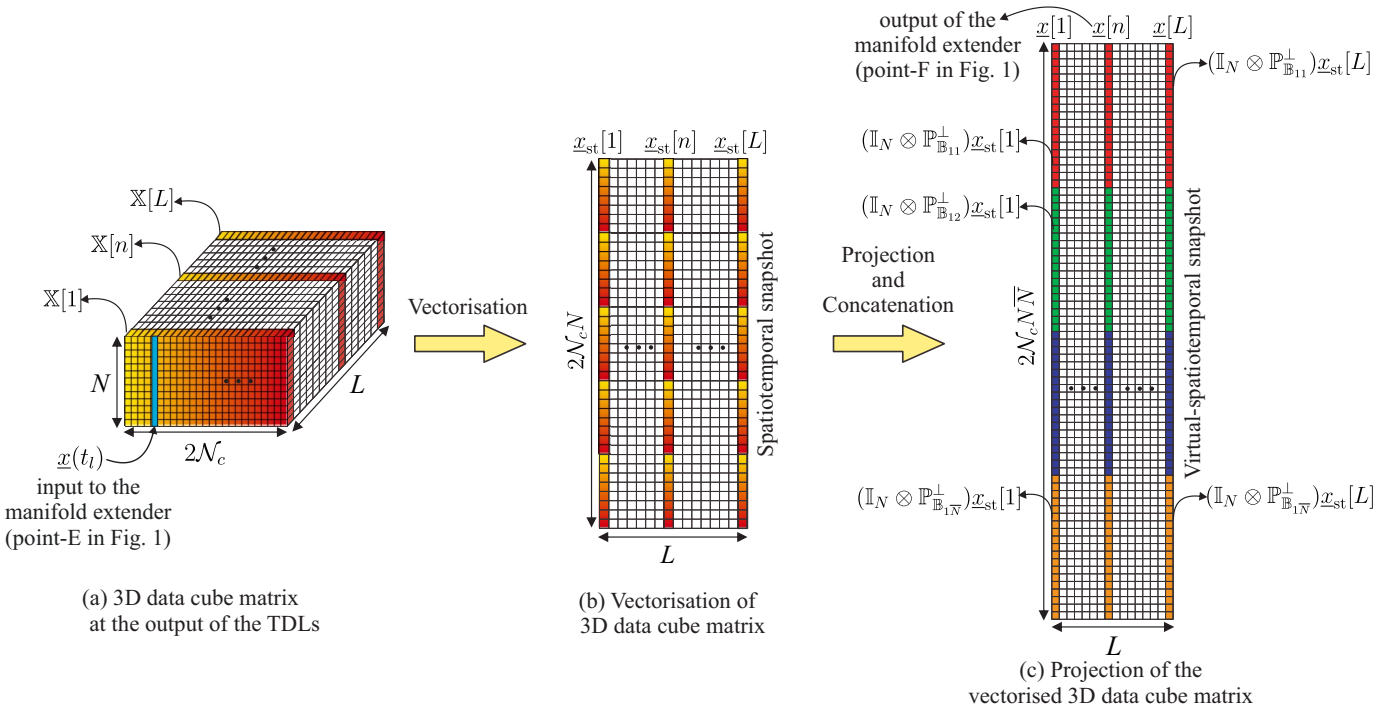

(a) 3D data cube matrix at the output of the TDLs

(b) Vectorisation of 3D data cube matrix

(c) Projection of the vectorised 3D data cube matrix

Fig. 3: Illustration of the received data processing at the manifold extender for the proposed system. The received data cube matrices in (a) are first vectorised to get spatiotemporal snapshots in (b), and then each spatiotemporal snapshot is projected by $\overline{N}$ projection operators to form virtual-spatiotemporal snapshot in (c). Different colors in (c) represent different projection operators.

given as

$$\mathbb{P}^{\perp}_{\mathbb{B}_1} = \begin{bmatrix} \mathbb{I}_N \otimes \mathbb{P}^{\perp}_{\mathbb{B}_{11}}, & \mathbb{O}_{2N\mathcal{N}_c}, & \cdots, & \mathbb{O}_{2N\mathcal{N}_c} \\ \mathbb{O}_{2N\mathcal{N}_c}, & \mathbb{I}_N \otimes \mathbb{P}^{\perp}_{\mathbb{B}_{12}}, & \cdots, & \mathbb{O}_{2N\mathcal{N}_c} \\ \vdots & \vdots & \ddots & \vdots \\ \mathbb{O}_{2N\mathcal{N}_c}, & \mathbb{O}_{2N\mathcal{N}_c}, & \cdots, & \mathbb{I}_N \otimes \mathbb{P}^{\perp}_{\mathbb{B}_{1\overline{N}}} \end{bmatrix} \tag{16}$$

Based on Equation 16, Equation 12 can also be written in a more compact form as follows

$$\underline{x}[n] = \underbrace{\sum_{k=1}^{K_1} \beta_{1k} \exp(j2\pi \mathcal{F}_{1k} n T_{cs})\, \mathrm{a}_1[n]\, \mathbb{P}^{\perp}_{\mathbb{B}_1} \underline{h}_{ik}}_{\text{desired term}} + \mathrm{ISI} + \mathrm{MAI} + \underline{\mathrm{n}}[n] \tag{17}$$

which contains the desired symbol, the ISI, the MAI and the noise $\underline{\mathrm{n}}[n]$. From Equation 17 it is clear that the virtual-spatiotemporal snapshot $\underline{x}[n]$ is a function of the extended manifold vector $\underline{h}_{ik} \in \mathcal{C}^{2N\overline{N}\mathcal{N}_c \times 1}$, which is defined as

$$\boxed{\underline{h}_{ik} = (\overline{\underline{S}}^{*}_{ik} \otimes \underline{S}_{ik}) \otimes (\mathbb{J}^{l_{ik}} \underline{c}_i \odot \underline{\mathcal{F}}_{ik})} \tag{18}$$

and called as virtual-spatiotemporal manifold vector. The word "virtual" has been used because the Tx manifold vector $\overline{\underline{S}}_{ik}$ and Rx manifold vector $\underline{S}_{ik}$ form the "virtual" manifold vector $\overline{\underline{S}}^{*}_{ik} \otimes \underline{S}_{ik}$. In Equation 18 the vector $\underline{c}_i \in \mathcal{R}^{2\mathcal{N}_c \times 1}$ representing the sum of the weight code vector associated with each Tx antenna of the i-th user. That is

$$\underline{c}_i = \begin{bmatrix} \mathbb{C}_i \\ \mathbb{O}_{\mathcal{N}_c \times \overline{N}} \end{bmatrix} \underline{1}_{\overline{N}} \tag{19}$$

where the operation with a vector of 1's does the "summation". It is important to point out that, the theoretical covariance matrix $\mathbb{R}_{xx} \in \mathcal{C}^{2N\overline{N}\mathcal{N}_c \times 2N\overline{N}\mathcal{N}_c}$ of $\underline{x}[n]$ is

$$\mathbb{R}_{xx} = \mathcal{E}\left\{\underline{x}[n]\, \underline{x}^{H}[n]\right\} \tag{20}$$

while in practice, over an observation interval of L symbols, this matrix can be expressed as follows

$$\mathbb{R}_{xx} \simeq \frac{1}{L} \sum_{n=1}^{L} \underline{x}[n]\, \underline{x}^{H}[n] \tag{21}$$

In summary, by observing $\underline{x}[n]$ or $\mathbb{R}_{xx}$, the "manifold extender" increases the dimensionality of the signal observation space from N to $2N\overline{N}\mathcal{N}_c$ so that the degrees of freedom has been increased.

C. Joint DOA-DOD Estimation

Assume the delay and Doppler frequency of all the paths of the desired user are pre-estimated (e.g. using the approach proposed in [7]). Based on these parameters, the projection matrix $\mathbb{P}^{\perp}_{\mathbb{B}_1}$ is constructed and thus the virtual-spatiotemporal snapshot $\underline{x}[n]$ is formed by Equation 12 or Equation 17. Towards this, the projection operator $\mathbb{P}_{\mathrm{n_v}}$ onto the subspace

spanned by noise eigenvectors of the covariance matrix $\mathbb{R}_{xx}$ can be formed. We now employ the virtual-spatiotemporal manifold vector associated with the desired user as given by Equation 18 in conjunction with the following cost function to yield the DOA and DOD of the desired user's paths

$$(\underline{\theta}, \overline{\underline{\theta}}) = \arg \max_{\forall(\theta,\overline{\theta})} \xi(\theta, \overline{\theta}) \tag{22}$$

where $\xi(\theta, \overline{\theta})$ is defined as follows

$$\xi(\theta, \overline{\theta}) = \frac{\left(\mathbb{P}^{\perp}_{\mathbb{B}_1} \underline{h}(\theta, \overline{\theta})\right)^H \mathbb{P}^{\perp}_{\mathbb{B}_1} \underline{h}(\theta, \overline{\theta})}{\left(\mathbb{P}^{\perp}_{\mathbb{B}_1} \underline{h}(\theta, \overline{\theta})\right)^H \mathbb{P}_{\mathbf{n_v}} \mathbb{P}^{\perp}_{\mathbb{B}_1} \underline{h}(\theta, \overline{\theta})} \tag{23}$$

This is easy to be optimised by using a 2D search where the peaks of the cost function $\xi(\theta, \overline{\theta})$ correspond to the DOA and DOD of all paths of the desired user respectively.

III. Computer Simulation Studies

In this section the performance of the proposed algorithm is evaluated using computer simulation studies. Without any loss of generality, the Tx and Rx antenna array geometries are assumed as uniform circular arrays (UCAs) on the (x, y) plane with $\overline{N} = 7$ antennas on the Tx's side and $N = 9$ antennas on the Rx's side. Furthermore, an observation interval of $L = 200$ transmitted symbols is assumed. Table I provides some additional system simulation parameters. The DOAs and DODs are assumed to be randomly selected following uniform distributions between 0 to 360 degrees.

TABLE I: Simulation Parameters

Parameter	Value	Parameter	Value
M	4	T_c	0.1 ms
K	3	N	9
$\mathcal{N}_c$	31 chips	$\overline{N}$	7

As indicated in Table I, there are $M = 4$ users, which implies that the desired user operates in the presence of three other co-channel interferers with $K = 3$ multipaths per user. Therefore, it is assumed that the unknown DOA and DOD of the three paths of the desired user are $(280°, 30°)$, $(200°, 110°)$ and $(60°, 140°)$, respectively. Fig. 4 shows the results of the joint DOA-DOD estimation indicating that the peaks occur at the correct directions associated with the three paths of the desired user.

Consider again the simulation environment in Fig. 4, now it is assumed two of the three paths of the desired user have directions close together in space. That is, the DOA and DOD values of three paths are $(92°, 68°)$, $(90°, 70°)$ and $(60°, 90°)$. The results are illustrated in Fig. 5 which still show high accuracy with sharp and distinguishable peaks, indicating the superresolution capabilities of the proposed algorithm.

Furthermore, a key performance parameter for subspace based estimation approaches is the number of the snapshots L required to achieve a certain root mean square error (RMSE) at a specified signal to noise ratio (SNR). Figures 6 and 7 show the results of Monte-Carlo simulation studies illustrating the performance of the proposed estimation algorithm in terms of the RMSE of the DOD and DOA estimation versus the (SNR$\times L$), respectively. The number of snapshots L is fixed at 200 (corresponding to data collected over an observation interval of 200 symbols) and the SNR varies from -3dB to 36dB. The number of multipath per user is assumed to be 2. As expected (see Chapter 8 in [8]), the error in the estimation of DOA and DOD decreases with an increase in (SNR$\times L$). Thus, when the SNR is low, a high number of snapshots may be needed to resolve two transmitters which are close together in space.

Figures 6 and 7 also show the performance of the system comparison between the proposed virtual-spatiotemporal

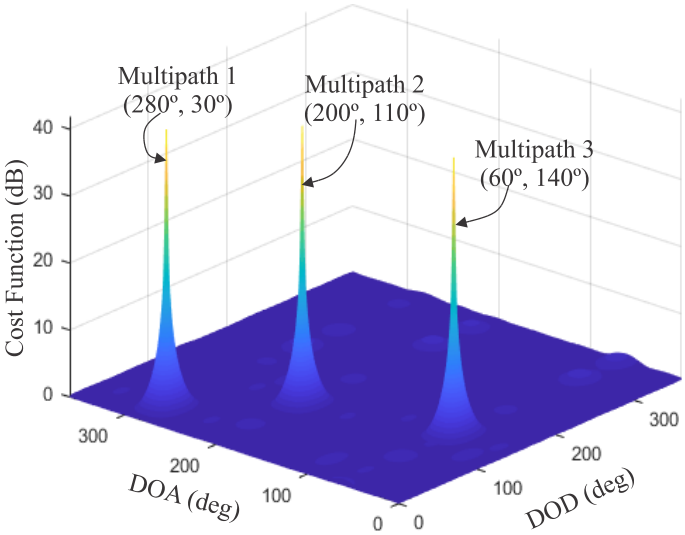

Fig. 4: Joint estimation of DOA and DOD corresponding to the three multipaths of the desired user.

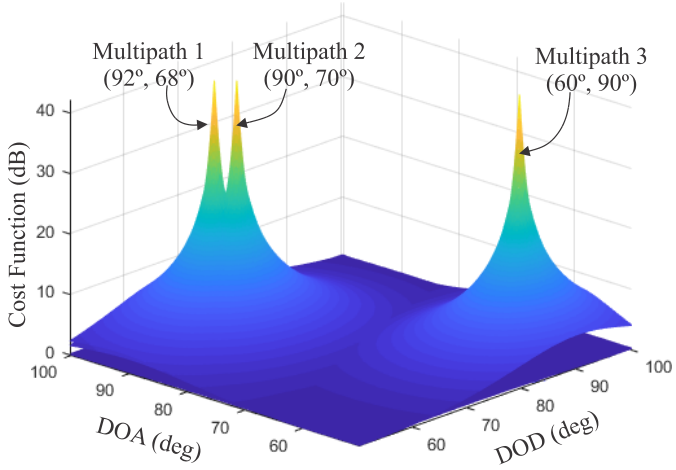

Fig. 5: Joint estimation of DOA and DOD when the signals from path 1 and path 2 of the desired user are closely spaced.

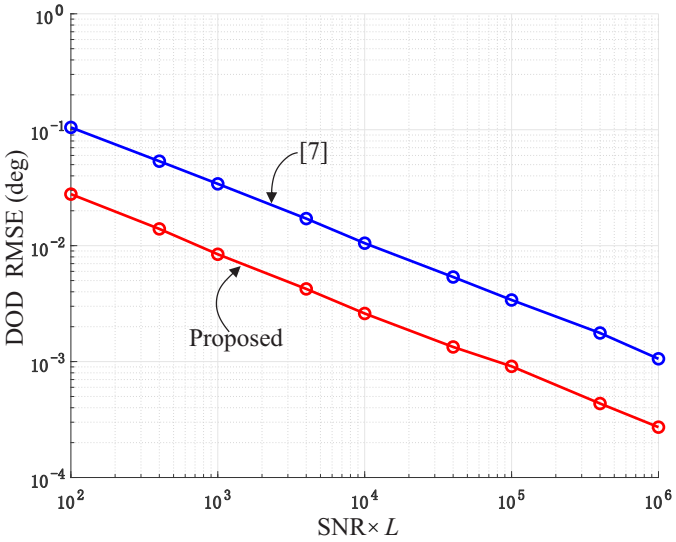

Fig. 6: RMSE of DOD estimation of the proposed algorithm (300 realisations). In the same plot, the performance of [7] is shown under the same environment.

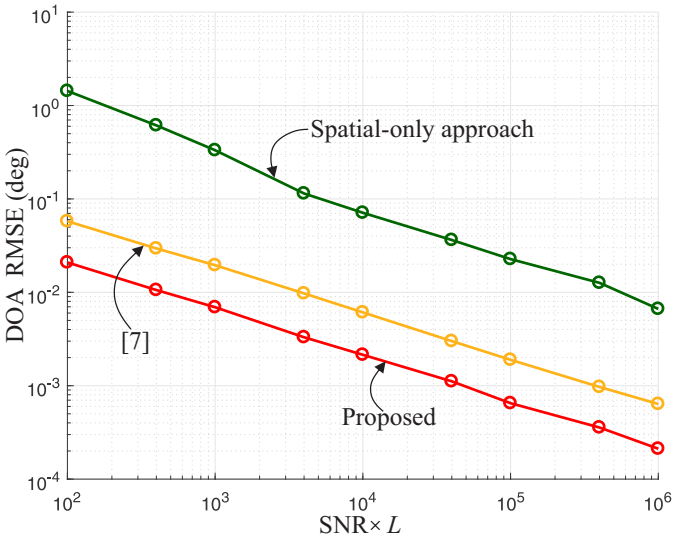

Fig. 7: RMSE of DOA estimation of the proposed algorithm (100 realisations). In the same plot, the performance of [7] and the spatial-only approach are shown under the same environment.

system, the virtual system [7] and the spatial-only system with the same Tx and Rx array geometries and under the same simulation environment. Note that the DOD estimation for the spatial-only system is not shown in Fig. 6 because such system cannot estimate the DODs as its Tx information cannot be exploited by the receiver. As illustrated in Fig. 6 and Fig. 7, the proposed system has superior channel estimation accuracy. It is also proven that the estimation accuracy is related to the dimensionality of the system (or degrees of freedom) since the dimensionality for the proposed virtual-spatiotemporal system, the virtual system and the spatial-only system is $2N\overline{N}\mathcal{N}_c > N\overline{N} > N$, based on the parameter value in Table I.

Note that to increase the DoF of the system, the spatial-only approach needs to increase the number of Rx antennas N to a large value in the order of 100s-1000s (Massive MIMO) [9]. Remember that massive MIMO approach requires more hardware (massive number of RF units, antennas, etc.) to create a massive N-dimensional observation space, while the approaches based on the "manifold extender" concept, like the one presented in this paper, keeps $N = \text{small}$ but creates a massive $N N_{\text{ext}}$-dimensional observation space by increasing the N_{ext} parameter which in our paper is $2\mathcal{N}_c\overline{N}$. This increases the DoF from N to $N N_{\text{ext}}$ and consequently improves the capabilities of the overall system.

IV. Conclusion

In this paper, a novel MIMO antenna array system was proposed which incorporates a virtual-spatiotemporal manifold extender to perform joint estimation of DOD and DOA of all multipaths of the desired user in the presence of multiple access co-channel interference. The proposed system largely increases the degrees of freedom by extending its system dimensionality with a fixed number of antennas. Finally, the proposed DOD and DOA estimation approach was evaluated with varying noise levels and compared against other estimation approaches. Computer simulation studies illustrated that the proposed approach outperforms the existing approaches.

References

[1] Z. Chen and A. Manikas, "Direction-of-Departure Estimation using Cooperative Beamforming," in *International Symposium on Wireless Communication Systems*, 2010, pp. 120–124.

[2] R. Pöhlmann, S. Zhang, A. Dammann, and P. A. Hoeher, "Manifold Optimization Based Beamforming for DoA and DoD Estimation with a Single Multi-Mode Antenna," in *European Signal Processing Conference (EUSIPCO)*, 2021, pp. 1841–1845.

[3] L. Hao, J. Rodríguez-Piñeiro, X. Cai, X. Yin, J. Hong, G. F. Pedersen, and S. Schwarz, "Measurement-based Double-Directional Polarimetric Characterization of Outdoor Massive MIMO Propagation Channels at 3.5GHz," in *IEEE 21st International Workshop on Signal Processing Advances in Wireless Communications (SPAWC)*, 2020, pp. 1–5.

[4] B. H. Fleury, M. Tschudin, R. Heddergott, D. Dahlhaus, and K. Ingeman Pedersen, "Channel Parameter Estimation in Mobile Radio Environments using the SAGE Algorithm," *IEEE Journal on Selected Areas in Communications*, vol. 17, no. 3, pp. 434–450, Mar. 1999.

[5] A. Richter, D. Hampicke, G. Sommerkorn, and R. S. Thoma, "Joint Estimation of DoD, Time-Delay, and DoA for High-Resolution Channel Sounding," in *IEEE 51st Vehicular Technology Conference Proceedings*, vol. 2, 2000, pp. 1045–1049.

[6] D. Zhu, J. Choi, and R. W. Heath, "Two-Dimensional AoD and AoA Acquisition for Wideband Millimeter-Wave Systems With Dual-Polarized MIMO," *IEEE Transactions on Wireless Communications*, vol. 16, no. 12, pp. 7890–7905, Dec. 2017.

[7] Z. Tang and A. Manikas, "DOA and DOD Channel Estimation in MIMO Access Networks," in *IEEE International Conference on Communications (ICC)*, May 2019, pp. 1–6.

[8] A. Manikas, *Differential Geometry In Array Processing*. Imperial College Press, 2004.

[9] B. Panzner, W. Zirwas, S. Dierks, M. Lauridsen, P. Mogensen, K. Pajukoski, and D. Miao, "Deployment and Implementation Strategies for Massive MIMO in 5G," *IEEE Globecom Workshops, GC Wkshps*, pp. 346–351, 2014.